



Results of 3-D georadar surveying and trenching the San Andreas fault near its northern landward limit

Alan Green^{a,*}, Ralf Gross^a, Klaus Holliger^a, Heinrich Horstmeyer^a, John Baldwin^b

^a*Institute of Geophysics, ETH-Hoenggerberg, CH-8093 Zurich, Switzerland*

^b*William Lettis and Associates, Inc., 1777 Botelho Drive, Suite 262, Walnut Creek, CA 94596, USA*

Received 29 June 2002; accepted 10 March 2003

Abstract

As part of a program to determine the location and geometry of the San Andreas Fault (SAF) buried beneath shallow sediments near its northern landward limit, three >20-m-long parallel trenches were constructed at positions distributed over a distance of ~ 55 m. The majority of excavated material comprised unconsolidated fluvial sediments deposited in a number of paleochannels. Single zones of active faulting identified in each of the trenches were initially interpreted in terms of a solitary strand of the SAF. To map the SAF between and beyond the trenches and to detect other active fault zones hidden by the young sedimentary cover, we collected a dense ground-penetrating radar (georadar) data set across a 23.2×72 m area. The data were recorded using a semi-automated acquisition system that included a conventional georadar unit coupled to a self-tracking laser theodolite with automatic target recognition capabilities. Since these data were plagued by system ringing as a result of the moderate-to-high electrical conductivities of the surficial sediments, an extensive data processing scheme was required to extract meaningful subsurface information. The final processed georadar volume (cuboid) contained numerous subhorizontal and trough-shaped reflections that originated from the fluvial paleochannels. Using the geological interpretation of the trench walls as a guide to pick semi-automatically the times of the most important reflecting horizons, we discovered that alignments of the nearly linear boundaries of these horizons defined two NW–SE trending strands of the SAF within the survey area. The georadar expression of the eastern SAF strand could only be traced over a distance of ~ 38 m. It had been intersected in the northern trench. In contrast, the western SAF strand extended over the entire length of the georadar volume and had been intersected in the central and southern trenches. Prominent reflections on georadar cross sections were found to be vertically displaced by 0.2–0.3 m across both SAF strands. A conspicuous linear-trending feature observed on horizontal sections at 3.3–3.6 m depth was laterally offset by 4.5–5.5 m along the eastern SAF strand. The interpreted vertical and horizontal offsets could have been generated by the 1906 San Francisco earthquake and/or earlier events. Undetermined amounts of aseismic slip may also have occurred along the newly defined SAF strands.

© 2003 Elsevier Science B.V. All rights reserved.

Keywords: 3-D georadar; San Andreas fault; Trenching; Paleoseismology

1. Introduction

Patterns of recent and historical seismicity are the basis for most methods of assessing seismic hazard. Critical data required for the construction of seismic

* Corresponding author. Tel.: +41-1-633-2657; fax: +41-1-633-1065.

E-mail address: alan@aug.ig.erdw.ethz.ch (A. Green).

hazard maps include the timing, magnitudes and hypocentral coordinates of earthquakes, the geometries of the active faults and the associated coseismic displacements. The reliability of seismic hazard maps depends on the accuracy of these seismological parameters and the completeness of the earthquake record. Under favorable circumstances, paleoseismological studies of the surface geomorphology and shallow subsurface geology may yield information that improves our knowledge of the seismological

parameters and extends the earthquake record back in time (McCalpin, 1996; Yeats et al., 1997). In addition to studying natural outcrops of soil, sediment and rock formations affected by earthquakes, it is common practice in paleoseismology to excavate trenches that provide appropriately oriented exposures of the shallow underground.

The well-known San Andreas Fault (SAF) is a dextral transform fault that juxtaposes the North American and Pacific tectonic plates (Fig. 1). Its

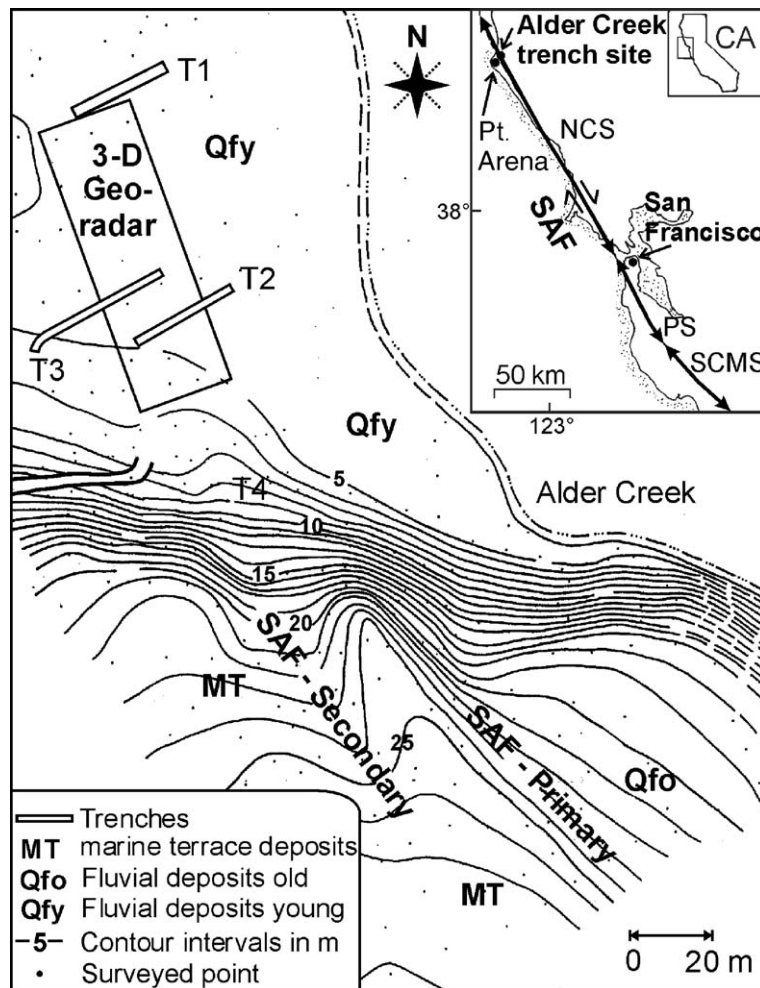


Fig. 1. Alder Creek site showing 3-D georadar survey area. Site in California is displayed in insets. NCS: North Coast Segment; PS: Peninsula Segment; SCMS: Santa Cruz Mountains Segment. Contour pattern and physiographic units delineate two strands of San Andreas Fault (SAF) in southern part of main map. Georadar data were acquired across the northern part in an attempt to interpolate and extrapolate SAF strand(s) identified in trenches T1–T3. Georadar survey area was limited eastward by west-migrating bed of Alder Creek and westward by a major highway.

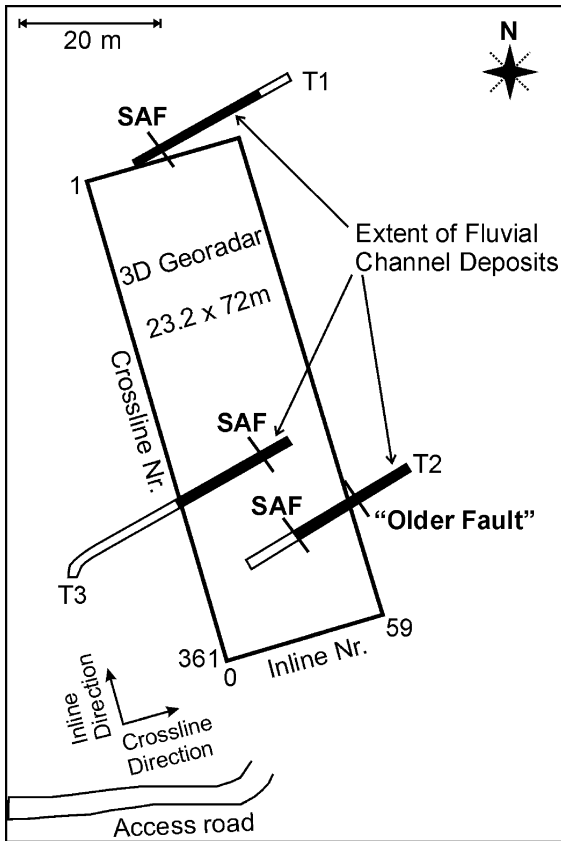


Fig. 2. Location of 3-D georadar survey with respect to trenches T1–T3 at Alder Creek. Limits of fluvial channel deposits and SAF strand(s) identified in trenches are outlined. An area of 1670.4 m² (23.2 × 72 m) was investigated with densely spaced georadar measurements. Final survey grid comprised 59 inline profiles and 361 crossline traces recorded with 0.2 m inline and 0.4 m crossline trace spacings.

Table 1

Acquisition parameters for 3-D georadar survey

| Acquisition parameter | 3-D survey |
|-----------------------|-------------|
| Antenna frequency | 200 MHz |
| Antenna separation | 0.75 m |
| Sample rate | 0.8 ns |
| Time window | 250 ns |
| Stacks/trace | 32 |
| Survey area | 72 × 23.2 m |
| In-line step size | 0.2 m |
| Crossline step size | 0.4 m |

character varies markedly along the length of western California. At some locations, it is a sub-meter wide fault zone, whereas at others, it includes several subparallel fault strands that together extend over widths of several kilometers (Working Group on California Earthquake Probabilities, 1999). To obtain information on past earthquakes that have affected the SAF close to its northern landward extremity, Baldwin (1996) investigated the Alder Creek site near Point Arena, which is approximately 225 km north of San Francisco (Fig. 1). Examination of tectonically induced geomorphological features, interpretation of aerial photographs and mapping of the shallow geology exposed in trenches yielded valuable but incomplete details on the complex geometry of the SAF at this site. To obtain a more comprehensive understanding of the active faulting that has affected this region, we have acquired a large 3-D (ground-penetrating radar) georadar data set that includes the area sampled by the trenches.

Over the past 10 years, georadar has been used to map the locations of fractures and faults in diverse

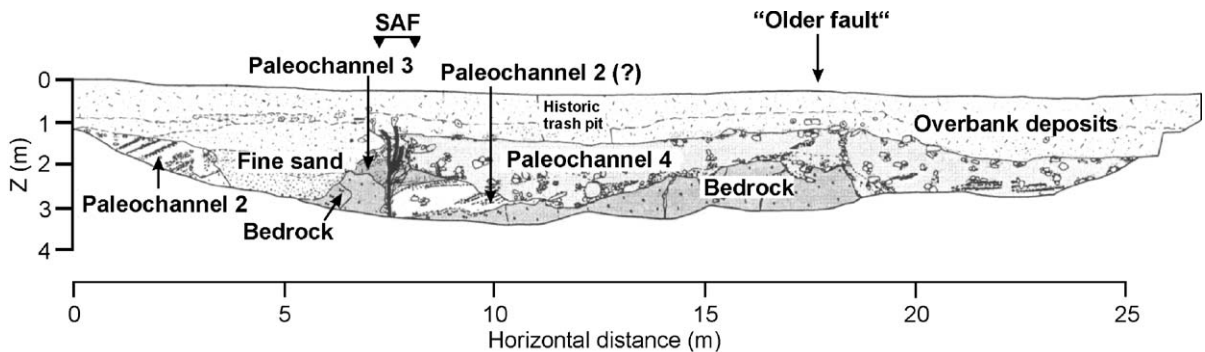


Fig. 3. Geology mapped on north wall of trench T2 showing dominant fluvial sedimentary units interrupted by “flower structure” of SAF (simplified from Baldwin, 1996). The “older” fault is best observed on south wall of trench.

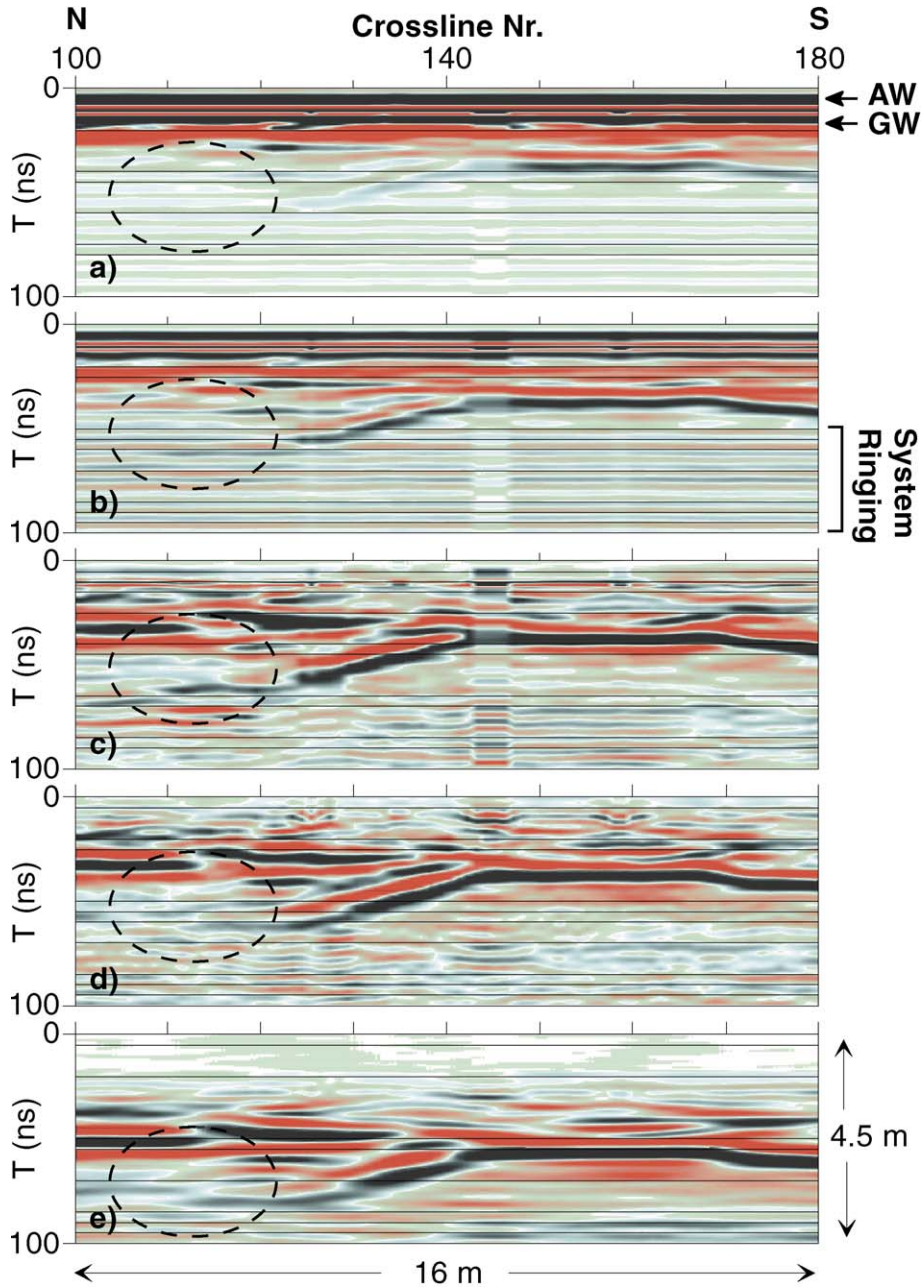


Fig. 4. Progressive results of applying processing scheme to a typical inline section extracted from 3-D georadar data set (see region highlighted by ellipse). (a) After dewow filtering and time-zero correction, data are dominated by direct air wave (AW) and ground wave (GW); (b) data are scaled with inverse of amplitude envelope (i.e. Hilbert transform) to reveal system ringing in lower part of section; (c) as for (b) after application of Karhunen–Loève filter; (d) as for (c) after 3-D phase-shift migration applied; (e) as for (d) after topographic correction and F-XY deconvolution. Blacks/blues and reds/oranges define positive and negative pulses and color intensity is a function of amplitude.

geological settings. For example, two-dimensional (2-D) georadar profiling has been used with limited success to examine the active Wasatch Fault in Utah (Smith and Jol, 1995) and the SAF in the San Francisco Bay region (Cai et al., 1996). Unfortunately, isolated 2-D profiles may not be sufficient for determining the geometries of faults in regions distinguished by highly heterogeneous subsurface structures. To map the shallow subsurface geology in such regions, Beres et al. (1995, 1999, 2000), Grasmück (1996), Grasmück and Green (1996) and others found it necessary to employ three-dimensional (3-D) georadar techniques.

After describing the geomorphology and near-surface geology at Alder Creek, we briefly explain our scheme for acquiring 3-D georadar data across a buried portion of the SAF. We then present key aspects of the georadar data processing and visualization strategies that were necessary to extract meaningful information about the dominant fluvial channel deposits and the buried strands of the SAF. When combined with information provided by the paleoseismological trenches, it is possible to trace two distinct NW–SE trending SAF strands across the georadar survey area. From the georadar data, we can also estimate the horizontal slip that has occurred along the eastern SAF strand and vertical displacements that have affected both strands within this region.

2. Local geomorphology and geology

Alder Creek is located along the North Coast Segment of the SAF (Fig. 1), which has been relatively aseismic since the magnitude 7.8 San Francisco earthquake of 1906 (Castillo and Ellsworth, 1993). The principle goal of Baldwin's (1996) paleoseismic investigation at Alder Creek was to determine the timing and magnitudes of past earthquakes and associated coseismic slips that have affected this northernmost region of the SAF. He observed two active strands of the SAF in the southern part of the study site. The primary SAF strand juxtaposes marine deposits in the west against Holocene fluvial sediments in the east, whereas the secondary strand cross-cuts the marine deposits (Fig. 1). Both fault strands can be traced northward to near the base of a steep erosional escarpment, across which the surface eleva-

tion drops by >20 m. A sequence of post-1906 overbank and other fluvial deposits of the shifting Alder Creek mask any evidence for active faulting across the topographically lower northern part of the site.

In an attempt to trace their northward extensions beneath the overbank deposits, Baldwin (1996) excavated three trenches T1–T3 normal to the trend of the two observed SAF strands (Figs. 1 and 2). Similar stratigraphic and structural features were observed in all trenches. For example, trench T2 exposes ~ 1 m of overbank deposits overlying two paleochannels (marked paleochannels 2 and 4 in Fig. 3) of Alder Creek that appear as 1.0- to 1.5-m-thick coarse gravel units incised into a bedrock of weathered Franciscan serpentinite. These paleochannels trend NW–SE, sub-parallel to the SAF. A 1.2-m-wide strand of the SAF was identified in trench T2 as a “flower structure” that truncated and offset the paleochannels and bedrock. It extends from the base of the overbank deposits to the bottom of the trench. Careful interpretation of small-scale structures suggests that three earthquakes separated by several hundred years have affected this fault zone (Baldwin, 1996). Toward the eastern end of trench T2, a seemingly inactive “older fault” that does not displace the fluvial sediments was observed.

A similar single near-vertical zone of recent faulting was observed in the other two trenches. Baldwin (1996) assumed that the fault zones observed in the three trenches were part of a single SAF strand and that the youngest deformation along this strand occurred during the 1906 San Francisco earthquake. Nevertheless, questions concerning the geometry of the SAF strands between and beyond the trenches and

Table 2
3-D georadar data processing sequence

| Processing sequence |
|--|
| Dewow |
| Bin traces |
| Stack data on regular grid |
| Time-zero correction |
| Amplitude scaling based on Hilbert transform |
| Karhunen–Loève filter |
| 3-D phase-shift migration |
| Topographic correction |
| F-XY deconvolution |

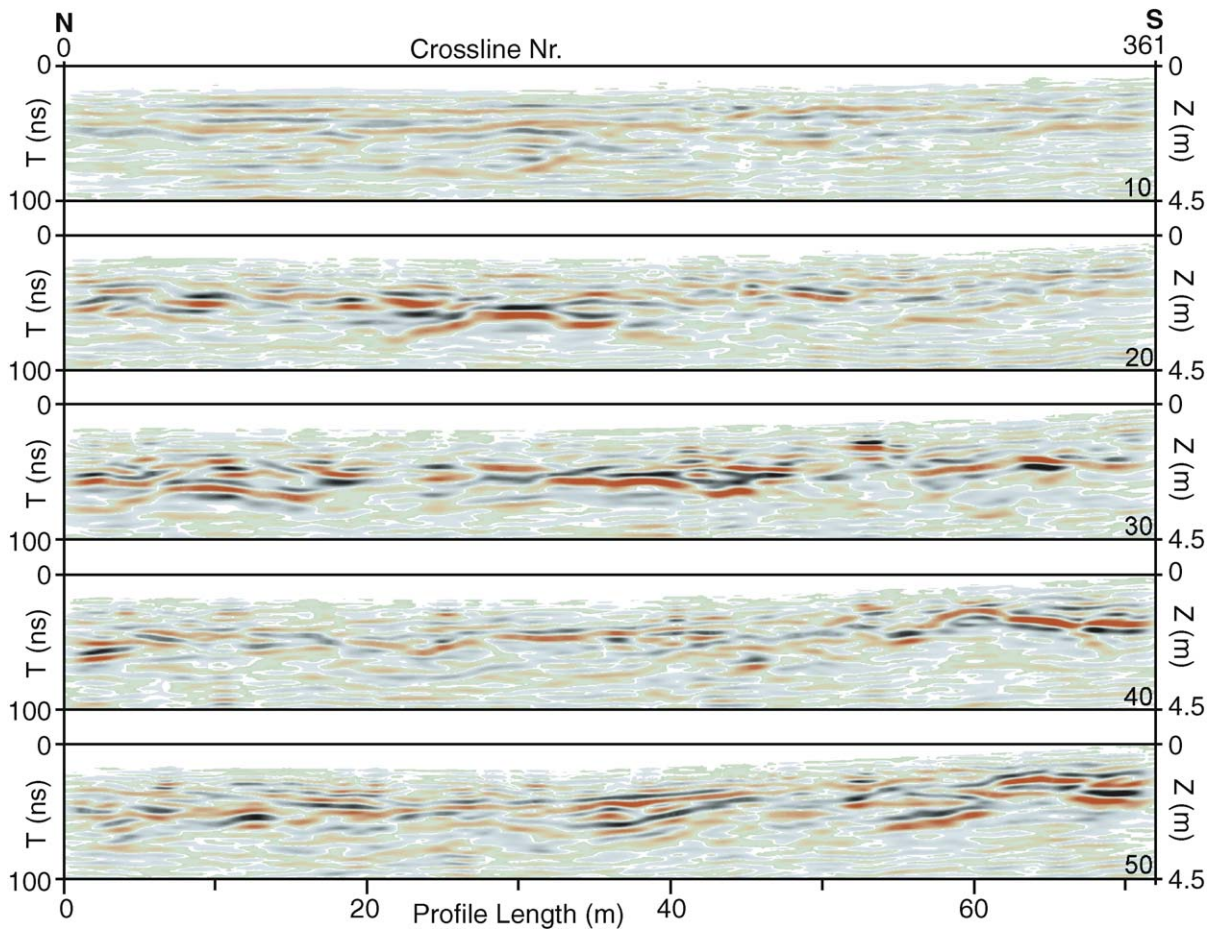


Fig. 5. Inline sections 10–50 extracted from 3-D georadar data set at 4-m intervals. Vertical/horizontal exaggeration is $\sim 2:1$. By displaying data subparallel to SAF, areas of different reflection strength and continuity are highlighted. Blacks/blues and reds/oranges define positive and negative pulses and color intensity is a function of amplitude.

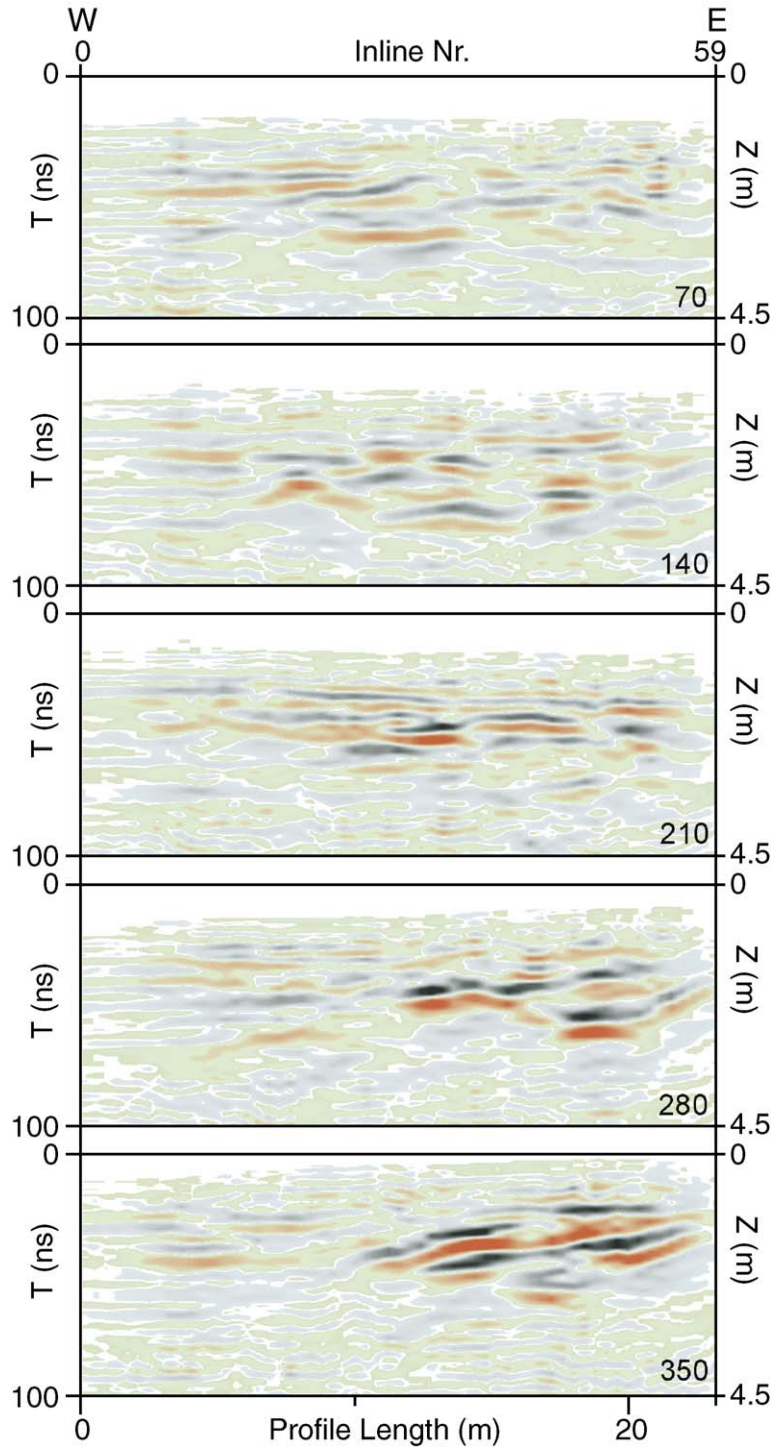
the presence of undetected secondary faults were left unanswered at this stage of the investigation.

3. Three-dimensional georadar data acquisition and processing

To study the region crossed by the northward projection of the primary SAF strand and the active fault zones exposed in the trenches, an area of

23.2×72 m was selected for 3-D georadar surveying (Figs. 1 and 2). We employed 200-MHz antennas separated by 0.75 m (Table 1). Our semi-automated acquisition system, which comprises a standard georadar unit linked to a self-tracking laser theodolite with automatic target recognition capabilities (Lehmann and Green, 1999), allowed us to collect dense 3-D georadar data across the entire survey area in a cost-effective manner. Subsequently, the field data were sorted into 0.40×0.80 m bins regularly spaced at

Fig. 6. Crossline sections 70–350 extracted from the 3-D georadar data set at 14-m intervals. Vertical/horizontal exaggeration is $\sim 2:1$. By displaying data perpendicular to SAF, changes in reflection patterns and truncations and/or offsets of reflections may indicate geologic disturbances in the shallow subsurface. Without further information, the SAF cannot be unambiguously located. Blacks/blues and reds/oranges define positive and negative pulses and color intensity is a function of amplitude.



0.2 × 0.4 m intervals, such that all traces contributed to more than one bin and neighboring bins overlapped. Considering that 32 measurements (vertical stacks) were summed in the field to yield the recorded traces and that bins generally contained eight traces or more (Table 1), the final stacked traces in most bins represented a composite of ≥ 256 measurements.

Stacking the traces in each bin yielded an initial georadar data volume dominated by direct air and ground waves at early times (Fig. 4a) and system ringing at later times (Fig. 4b). Low-energy system ringing is a characteristic of georadar data sets recorded across moderately to highly conducting fine-grain sediments. Vertical and horizontal sections extracted from the initial georadar volume revealed few discernible subsurface reflections. To improve the

ratio of useful signal to source-generated noise, it was necessary to apply a range of processing steps to the georadar data (Table 2; Fig. 4).

Each trace was first divided by a smoothed version of its Hilbert transform (amplitude envelope) to increase the amplitudes of later arrivals relative to those of earlier ones (Fig. 4b). Karhunen–Loève multichannel filtering (Jones and Levy, 1987) then effectively eliminated the air and ground waves as well as the system ringing. After this processing step, numerous georadar reflections and diffractions from subsurface structures were revealed (Fig. 4c). Subsequently, application of a 3-D phase-shift migration algorithm using a constant velocity of 0.09 m/ns (determined from extensive migration tests and low quality expanding-spread data) moved dipping reflec-

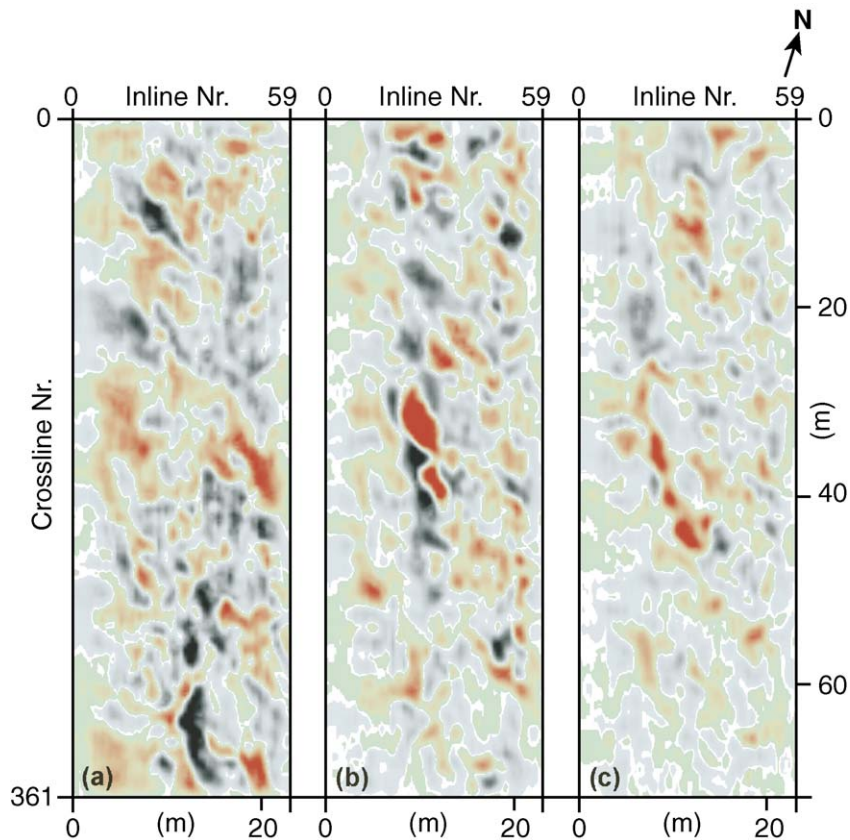


Fig. 7. Horizontal sections (timeslices) extracted from 3-D georadar data set at (a) 45, (b) 55 and (c) 65 ns. Patterns show lateral extent of reflections. NW–SE trending features indicate paleo-Alder Creek flow direction and/or fault-related structures. Without further information, the SAF cannot be unambiguously located. Blacks/blues and reds/oranges define positive and negative pulses and color intensity is a function of amplitude.

tions to their correct positions, unraveled crossing events and collapsed diffractions (Fig. 4d). Final processing involved time-shifting each trace to a common horizontal datum and passing the entire georadar volume through an F-XY deconvolution routine to reduce incoherent noise (Fig. 4e; Canales, 1984).

4. Data presentation

Fig. 5 shows regularly spaced inline sections 10, 20, 30, 40 and 50 extracted from the georadar volume. Maximum depth penetration is generally ~ 4.5 m (~ 100 ns). These complex images reveal numerous interfingering and crosscutting structures and several trough-shaped features. Laterally continuous reflections are observed at various depths and positions. Most are undulating with apparent inclinations varying from subhorizontal to gently north and gently south dipping. All sections contain reflections that can

be traced over distances >10 m, with many having lengths of 18–25 m. Since the inline profiles are subparallel to the general direction of the SAF, evidence for recent faulting is not expected in these images.

Evenly spaced crossline sections 70, 140, 210, 280 and 350 displayed in Fig. 6 are approximately normal to the regional trend of the SAF. They display structures that are similar in many ways to those represented on the inline sections, except they contain fewer laterally continuous reflections (this may be influenced by the shorter lengths of the sections). Although there are a number of locations at which reflections are truncated or offset, it is not possible without further information to identify unambiguously the SAF strands on these sections.

The 45, 55 and 65 ns horizontal sections (time-slices) presented in Fig. 7 highlight the complexity of structures underlying the Alder Creek site at three different depths. All reveal a dominant NW–SE trending fabric, subparallel to the present and former

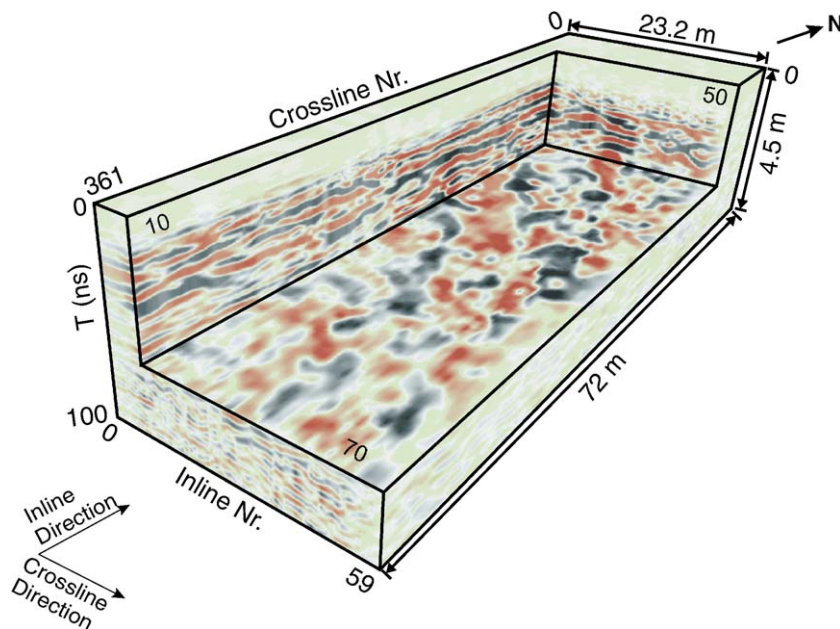


Fig. 8. Internal view of 3-D georadar block. The georadar volume was cut along inline 10, crossline 50 and 70 ns horizontal section (timeslice) to illustrate general data quality as well as lateral and vertical dimensions of structures. Although reflections on inline section are quite complex, they show a high degree of lateral continuity. The crossline section, which is nearly perpendicular to the SAF, reveals abrupt changes and truncations of reflections. NW–SE trending features on horizontal section indicate paleo-Alder Creek flow direction and/or fault-related structures. Without further information, SAF cannot be unambiguously located. Blacks/blues and reds/oranges define positive and negative pulses and color intensity is a function of amplitude.

Alder Creek flow directions and the SAF. There are a number of structures that extend >20 m in this direction and there is evidence for much longer lineaments (e.g. crosscutting features near the center of Fig. 7b). Nevertheless, the majority of features are relatively small, with dimensions <10 m. Without constraints from geological or other geophysical data, it is not possible to distinguish between fluvial- and tectonic-related structures in the georadar patterns of Fig. 7.

When vertical and horizontal sections are combined and displayed from different directions, the 3-D geometries and sizes of important structures can be conveniently examined. Fig. 8 shows a perspective view of arbitrary vertical and horizontal sections. On this and similar composite 3-D figures, it is possible to establish the location, shape and size of a wide variety

of features. The significance of some structures only becomes apparent when viewed in three dimensions. For example, careful examination of 3-D images demonstrates that NW–SE elongated subhorizontal and trough-shaped reflections extending over distances in excess of 15–20 m are the most conspicuous structures in the Alder Creek georadar volume. Once identified on such 3-D plots, semi-automatic routines can be used to pick the surfaces and boundaries that define the critical geological structures.

5. Interpretation

Faults and fault zones produce a variety of signatures on georadar data according to antenna frequency and orientation, heterogeneity of the faulted material

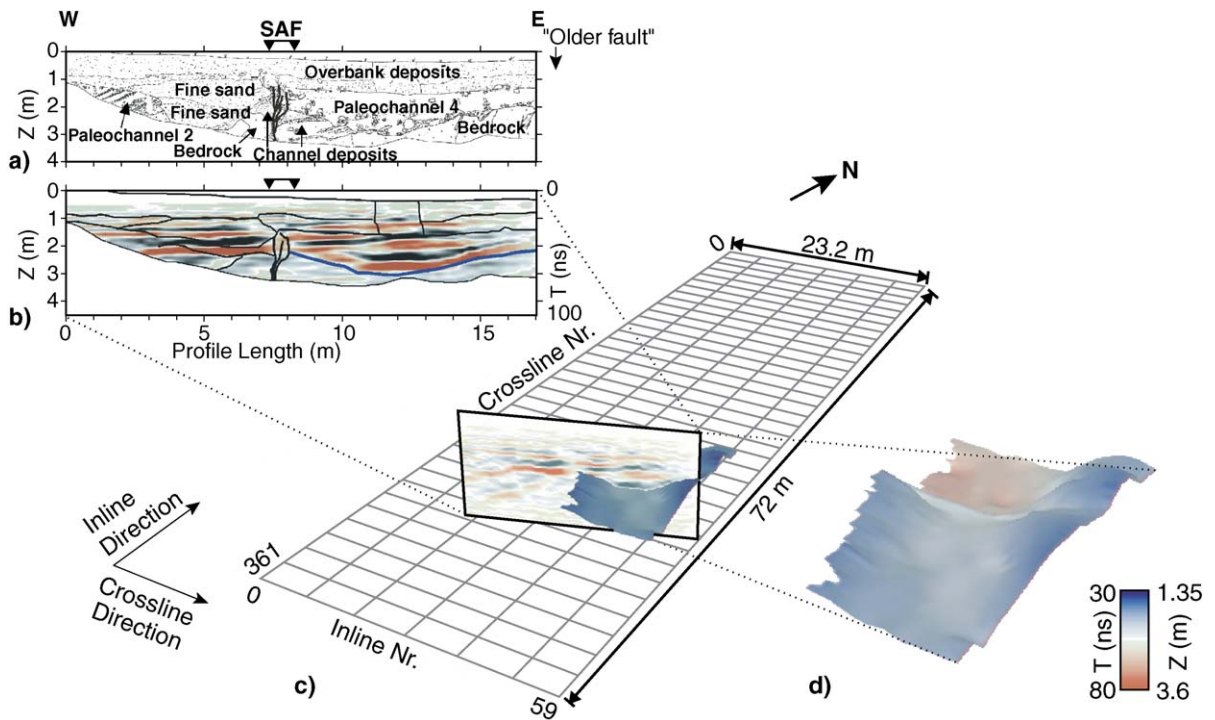


Fig. 9. (a) Geology mapped on a portion of trench T2 north wall showing fluvial sedimentary units interrupted by SAF “flower structure” (simplified from Baldwin, 1996). (b) Oblique georadar cross section (extracted from georadar volume) parallel to, but offset to the north from trench T2 by ~ 1.5 m. Geological boundaries and fault strand mapped in trench are superimposed. Discontinuities in central part of georadar cross section correlate with SAF “flower structure”. Blacks/blues and reds/oranges define positive and negative pulses and color intensity is a function of amplitude. (c) Perspective view of semi-automatically picked reflecting horizon that represents base of Alder Creek paleochannel 4 identified in the trench. (d) Zoomed version of (c) shows better the geometry of reflecting horizon, which is truncated to west by the western SAF strand (rugged western edge of the reflecting horizon is the result of event terminations, whereas smooth eastern edge delineates the boundary of the data). Travel time and depth to picked horizon is colour-coded.

and the dip and length of the rupture zone (Beres et al., 2000; Lehmann et al., 2000). Taking these points into account and after careful examination of all vertical and horizontal sections, we conclude that the SAF strands cannot be located on the basis of georadar data alone. As a consequence, we begin our interpretation by calibrating the georadar data with the geology mapped on the walls of the excavated trenches.

Fig. 9b shows an oblique georadar cross section extracted from the georadar volume parallel to trench T2, but offset from it to the north by ~ 1.5 m. The relevant portion of the trench log from Fig. 3 is reproduced in Fig. 9a. For detailed correlation, the geological boundaries and the fault zone defined by the trench log are superimposed on the georadar section. These figures demonstrate that significant reflections are associated with the base of the over-bank deposits and with the upper and lower boundaries of Alder Creek paleochannel 4. Furthermore,

distinct disruptions of georadar reflections over a 1- to 2-m-wide zone delineate the SAF strand at lateral position 7.5 m. It truncates reflections that originate from the paleochannel boundaries to the east and a fine-grain sand unit to the west. Poor correlations between other parts of the georadar image and the mapped geology are due to the ~ 1.5 m offset between the georadar section and trench and undocumented vertical and lateral velocity variations.

Semi-continuous reflections from the base of paleochannel 4 (marked blue in Fig. 9b) allow it to be semi-automatically picked (traced) over a wide area adjacent to trench T2 (Fig. 9c and d). Its axis is subparallel to the present Alder Creek flow direction and its western margin appears to be terminated along the northward projection of the SAF strand identified in trench T2, perhaps indicating that the ancient Alder Creek once crossed the SAF before being ruptured and offset. Because we are unable to identify the displaced portion of paleochannel 4 on the western

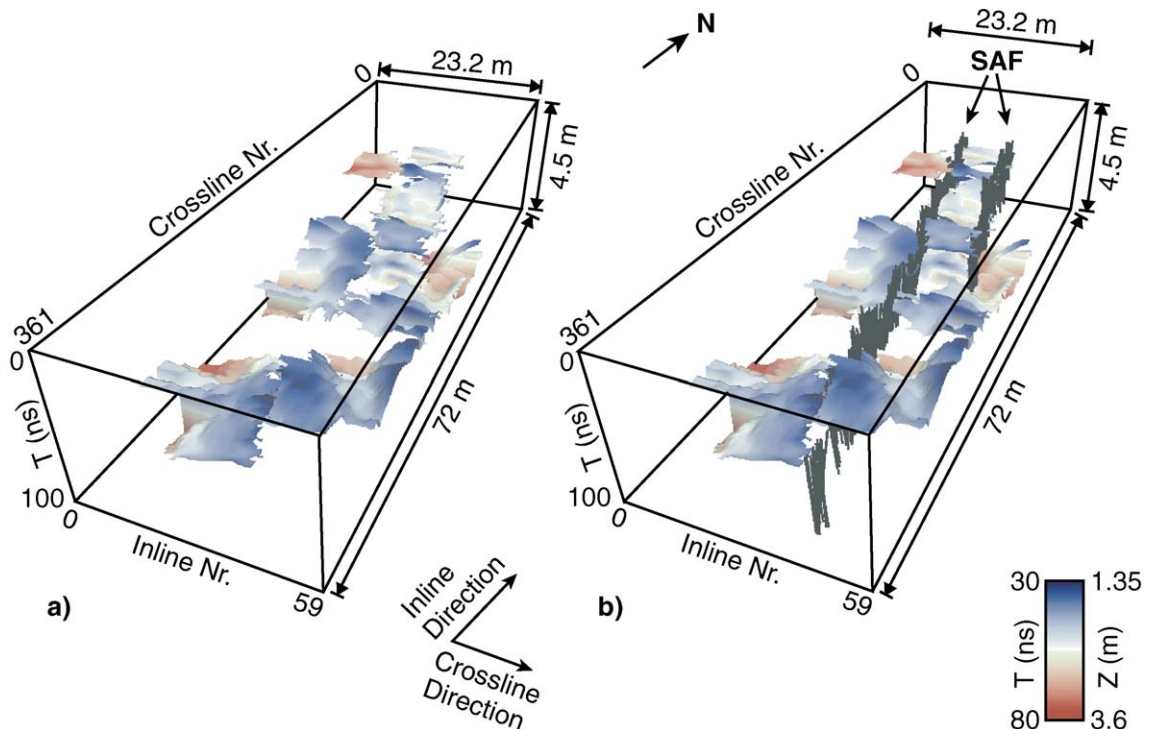


Fig. 10. (a) Semi-automatically picked reflecting horizons identified throughout georadar volume. Travel time and depth to picked horizon is colour-coded. (b) Alignments of truncations and offsets of reflecting surfaces shown by the near-vertical black lines define two SAF strands. Blacks/Blues and reds define positive and negative pulses and colour intensity is a function of amplitude. Figure taken from Gross et al. (2002).

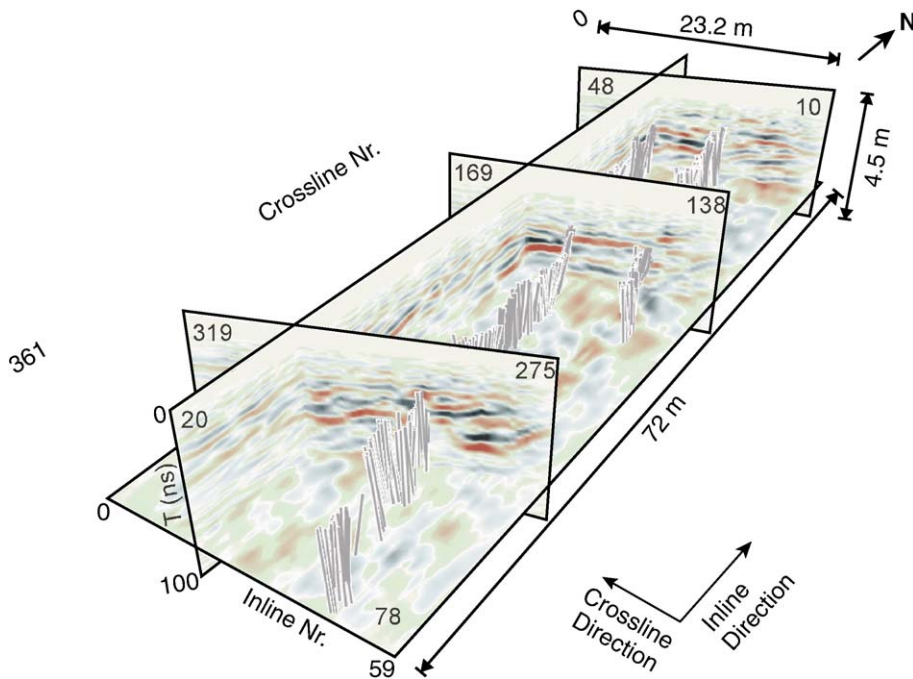


Fig. 11. Perspective view of two SAF strands superimposed on vertical and horizontal sections. Blacks/blues and reds/oranges define positive and negative pulses and color intensity is a function of amplitude.

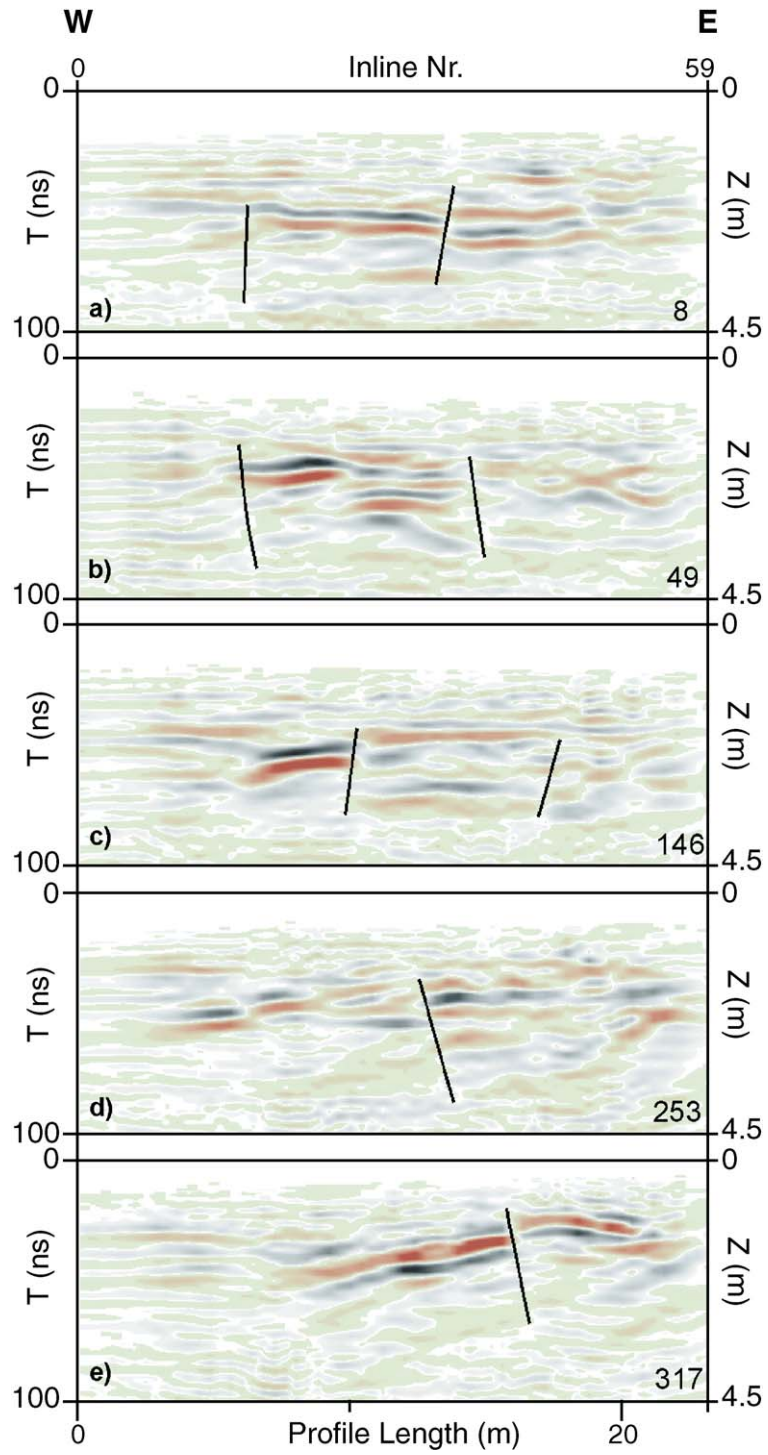
side of the survey area, we cannot determine the associated cumulative coseismic and aseismic slip.

Similar expressions of sedimentary stratigraphy and SAF strands were observed in the 3-D georadar data recorded adjacent to trenches T1 and T3. In particular, the subhorizontal and channel-like boundaries of several sedimentary units produced continuous reflections, whereas the SAF was represented by distinct changes in reflection pattern and terminations and/or apparent near-vertical offsets of laterally continuous reflections.

Even though SAF strands were clearly identified in the trenches and in adjacent regions of the georadar data, it was not an easy matter to trace the SAF strands over long distances through the georadar volume; several meters on either side of the trenches, the distinct georadar character of the SAF strands on the

crossline sections either faded or bifurcated. Since the trench logs demonstrated that the SAF truncated and offset formerly continuous sedimentary units, we decided to map the lateral extent of all important georadar reflecting horizons with emphasis on determining the locations and nature of their boundaries. Using a combination of vertical and horizontal sections and 3-D composite images (e.g. Figs. 5–8), we semi-automatically picked all reflections that had areal extents $>10 \text{ m}^2$. These subhorizontal and channel-like reflecting surfaces mostly trend NW–SE, parallel to the paleochannels mapped in the trenches (Figs. 9c,d and 10a). They likely represent primary and secondary fluvial structures that were terminated or ruptured during one or more erosional or tectonic events. On completing this exercise, we discovered that alignments of NW–SE trending linear truncations

Fig. 12. Georadar crossline sections 8, 49, 146, 253 and 317 showing two distinct SAF strands. Vertical to horizontal exaggeration is $\sim 2:1$. Eastern strand is observed in trench T1, whereas western strand is seen in T2 and T3. (a–c) Both fault strands are identified in northern and central parts of georadar survey area by areas of different reflection strength and character and by reflection truncations and offsets. (d, e) Only the eastern fault strand defined by reflection truncations and offsets is observed in southern part of georadar survey area. Blacks/blues and reds/oranges define positive and negative pulses and color intensity is a function of amplitude. Figure taken from Gross et al. (2002).



and offsets of the reflecting horizons (Fig. 10a) together with major disruptions of reflections (e.g. Fig. 9b) defined the locations of two SAF strands in our survey area (Fig. 10b). It is this definition of the two SAF stands that we employed in our interpretation.

Fig. 11 shows the two SAF strands extracted from Fig. 10b superimposed on a perspective view of the georadar data as expressed by arbitrary inline, crossline and horizontal sections. Both SAF strands can be identified in the northern part of the survey area. The eastern SAF strand correlates with the fault zone mapped in trench T1. It can be traced southeastward to near the eastern edge of the georadar volume at crossline section 190, where its physical expression gradually disappears. By comparison, the western

SAF strand extends along the entire length of the survey area. It is exposed in trenches T2 and T3.

Once the positions of the SAF strands were established, it was possible to estimate their approximate inclinations on many (by no means all) crossline sections. Abrupt changes in reflection pattern and truncations and offsets of reflecting horizons displayed on the selected crossline sections of Fig. 12 demonstrate the steep-dipping character of the two SAF strands. Considering the amount of processing that was required to derive the final georadar volume and the nearly random nature of the slight east- and west-directed dips shown in Fig. 12, our best estimate is that the SAF strands are vertical structures at shallow depths. On numerous crossline sections, reflections on either side of both SAF strands have

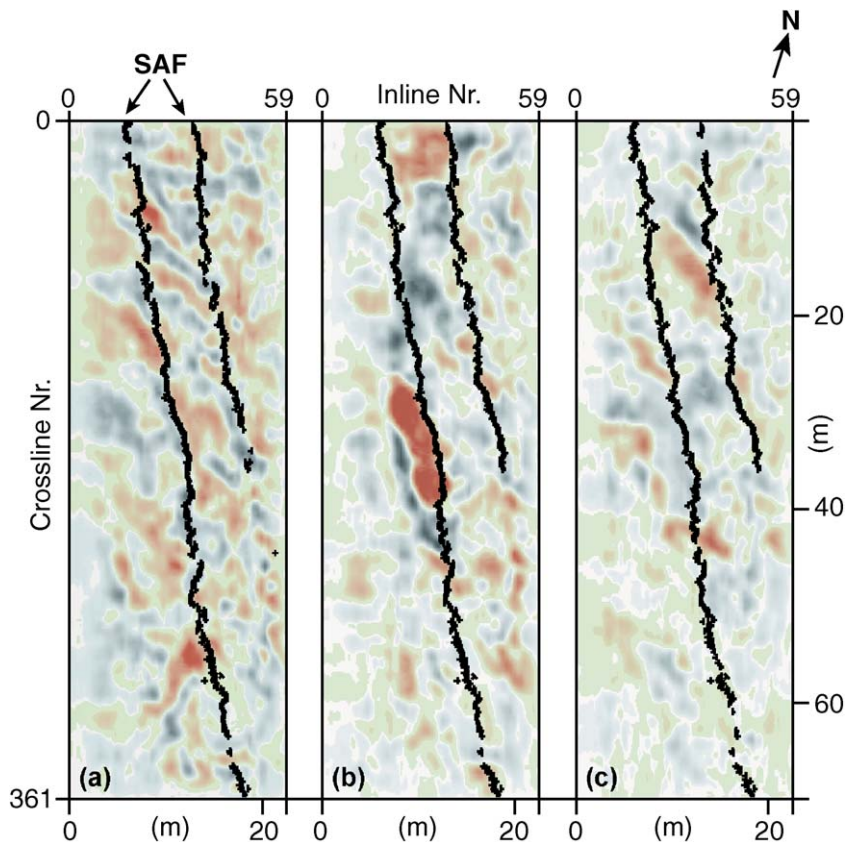


Fig. 13. Horizontal georadar sections (timeslices) at (a) 48, (b) 58 and (c) 68 ns showing locations of SAF at different depths. In northern and central parts of survey area, two distinct strands define the complicated SAF structures. Dominant NW–SE trending reflection patterns likely represent fluvial sedimentary units. Blacks/blues and reds/oranges define positive and negative pulses and color intensity is a function of amplitude.

apparent vertical offsets of 0.2–0.3 m. Similarly, small vertical displacements were reported at other locations of the SAF following the 1906 San Francisco earthquake (Lawson, 1908).

Careful analysis demonstrates that the SAF strands are responsible for distinct lineations on the horizontal georadar sections (Fig. 13), but they are rarely the most prominent features. As suggested previously, most of the subhorizontal and trough-shaped reflections that dominate the appearance of the horizontal sections are probably associated with NW–SE trending paleochannels of Alder Creek. Nevertheless, on horizontal sections in the 3.3–3.6 m depth range, a NW–SE trending feature is horizontally offset by 4.5–5.5 m along the eastern SAF strand (Fig. 14). Although there is no direct information on its stratigraphic character and age, we suspect that the displaced feature is a deep secondary paleochannel.

Clearly, we do not know when the offset depicted in Fig. 14 occurred. Regardless, any interpretation of active faulting at Alder Creek needs to account for the following:

- the offset in Fig. 14 is 0.2–0.5 m deeper than the deepest deformation of sediments observed in the trenches;

- the eastern SAF strand defined by the 3-D georadar data disrupts fluvial sediments in trench T1 (i.e. it is an active fault), but its georadar expression fades out southeastward as it approaches the “older fault” mapped in trench T2 (Figs. 2 and 3);
- the 4.5–5.5 m offset shown in Fig. 14 is close to the 4.9 m of dextral slip observed 1.2 km southeast of Alder Creek shortly after the 1906 earthquake (Lawson, 1908) and the 4.8–5.9 m of coseismic horizontal displacement estimated from triangulation data acquired near and adjacent to Point Arena (Thatcher et al., 1997);
- the western SAF strand, which can be followed along the length of the georadar volume and interrupts fluvial sediments in trenches T2 and T3 (i.e. it is also an active fault), appears to project southeastward to become the primary SAF identified at the surface in the southern part of the study site;
- Baldwin (1996) found evidence for the 1906 and two pre-1906 earthquakes in trench T2.

There are at least three plausible interpretations of the available information. (1) Somewhere near the center of the georadar survey area, the major component of movement during the 1906 earthquake stepped

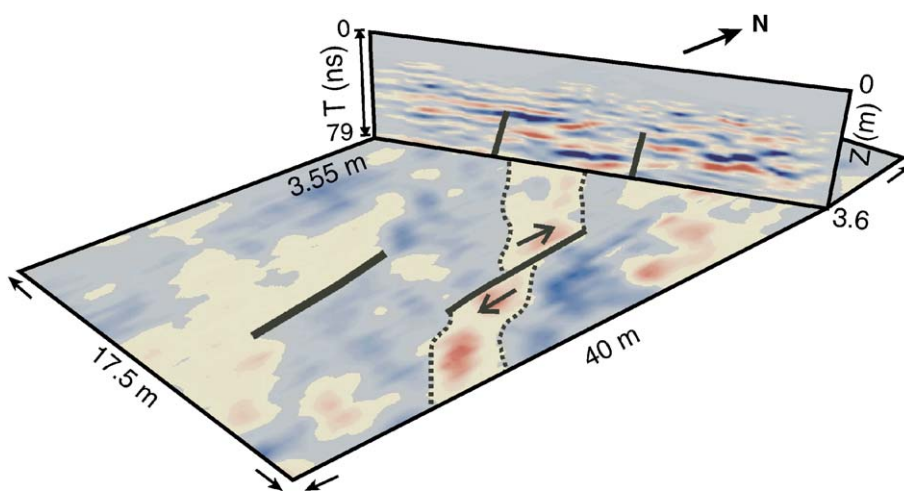


Fig. 14. Perspective view of northern part of georadar volume. Approximately 4.5–5.5 m of right-lateral fault movement offsets a distinct geological feature observed on the 79 ns (~ 3.6 m depth) horizontal section. Vertical section shows two fault strands that correspond to fault traces marked on horizontal section. Based on trench T1 information, offset feature is probably a minor paleochannel (now filled). Reds and blues define positive and negative pulses (opposite scheme to that used for other figure) and colour intensity is a function of amplitude. Figure taken from Gross et al. (2002).

eastward from the western to the eastern SAF strand. (2) Alternatively, coseismic displacements during the 1906 earthquake were concentrated along the western SAF strand and a significant pre-1906 event was responsible for the “older fault” and the offset of the relatively deep feature observed along the eastern SAF. (3) Finally, displacements along both SAF strands were the cumulative result of movements generated by the 1906 earthquake, earlier earthquakes and aseismic slip.

6. Conclusions

After trenching was completed at the Alder Creek paleoseismological study site in northern California, key questions concerning buried portions of the San Andreas Fault (SAF) near its northern landward extremity remained. For example, was Baldwin's (1996) initial interpretation of a single SAF strand running through all three trenches correct? Were there hidden SAF strands still to be discovered? What were the shallow geometries of the SAF strands and how much coseismic displacement was associated with them?

To address these issues, we acquired a dense 3-D georadar data set across a 23.2×72 m area that crossed or passed close to the three trenches (Figs. 1 and 2). Extensive processing of the georadar data (Table 2; Fig. 4) was required to remove the effects of the direct air and ground waves and eliminate system ringing caused by the moderate to high electrical conductivities of the surficial sediments. The final processed georadar volume contained prominent subhorizontal and trough-shaped reflections (Figs. 5–8) that originated from numerous fluvial paleochannels, some of which were encountered in the trenches (Fig. 9a and b). Despite the high quality of the final georadar volume, it was not possible to define confidently the locations and geometries of the SAF strands on the basis of these data alone.

We began our attempt to delineate the SAF strands by calibrating their georadar signatures with the active fault zones observed in the trenches. At each trench, the SAF strand was represented by abrupt terminations and offsets of reflections from the fluvial paleochannels. Unfortunately, these characteristic SAF signatures could not be confidently followed for more

than a few meters on either side of the trenches. Our next step involved semi automatically picking the times of the most important paleochannel reflecting surfaces. A map of reflecting surfaces that defined the locations, geometries and sizes of the paleochannels (Figs. 9c,d and 10a) was a key result of this time consuming task. The NW–SE trending outer boundaries of these surfaces were found to be approximately colinear. They delineated two SAF strands (Figs. 10b and 11), the eastern one of which had been exposed in trench T1 and the western one of which had been exposed in trenches T2 and T3. The eastern SAF strand extended southeastward from the northern edge of the georadar survey over a distance of ~ 38 m, whereas the western strand could be traced along the entire length of the georadar volume. It is noteworthy that the SAF strands observed at our study site (primary and secondary strands in the south, and eastern and western strands in the north) had a complex en échelon character, typical of ruptures in young unconsolidated sediments (Yeats et al., 1997). After the locations and geometries of the two SAF strands had been ascertained, we examined all crossline and horizontal georadar sections for evidence of vertical and horizontal displacements that may have occurred along the fault zones.

As shown in the crossline sections of Fig. 12, reflections appear to be vertically offset by 0.2–0.3 m across both SAF strands. Apparent vertical offsets of reflections could be due to horizontal movements of topographically undulating features or to vertical displacements. Since the SAF is known to have generated vertical movements of this magnitude within 1.7 km of the survey site (Lawson, 1908; Baldwin, 1996), we favour the latter interpretation. Horizontal sections between 3.3 and 3.6 m contain a conspicuous linear trending feature that is laterally offset by 4.5–5.5 m along the eastern SAF strand (Fig. 14). Although we found no evidence for similar offsets along the western SAF strand, our data do not preclude the large horizontal displacements required to explain the trenching observations of this fault zone (Baldwin, 1996). We do not know if the inferred and observed displacements on the SAF strands at Alder Creek are solely the result of the 1906 San Francisco earthquake. Coseismic displacements generated by earlier events and aseismic slip could also play a major role.

Acknowledgements

We thank the United States Geological Survey for logistic and other support. Funding for this project was provided by the Swiss National Science Foundation.

References

- Baldwin, J.N., 1996. Paleoseismic Investigation of the San Andreas Fault on the North Coast Segment, near Manchester, California. MSc Thesis, San Jose State University. 105 pp.
- Beres, M., Green, A.G., Huggenberger, P., Horstmeyer, H., 1995. Detailed 3-D georadar studies of glaciofluvial sediments. *Geology* 12, 1087–1091.
- Beres, M., Huggenberger, P., Green, A.G., Horstmeyer, H., 1999. A study of glaciofluvial architectures using two- and three-dimensional georadar methods. *Sediment. Geol.* 129, 1–24.
- Beres, M., Green, A.G., Pugin, A., 2000. Diapiric origin of the Chessel–Noville hills of the Rhone Valley interpreted from georadar mapping. *Environ. Eng. Geosci.* VI, 141–153.
- Cai, J.C., McMechan, G.A., Fisher, M.A., 1996. Application of ground penetrating radar to investigation of near-surface fault properties in the San Francisco Bay Region. *Bull. Seismol. Soc. Am.* 86, 1459–1470.
- Canales, L.L., 1984. Random noise reduction. 54th Ann. Internat. Mtg., Soc. Expl. Geophys., Expanded Abstract. Society of Exploration Geophysics, Tulsa, p. 525.
- Castillo, D.A., Ellsworth, W.L., 1993. Seismotectonics of the San Andreas fault system between Point Arena and Cape Mendocino in Northern California: implications for the development and evolution of a young transform. *J. Geophys. Res.* 98, 6543–6560.
- Grasmück, M., 1996. 3D ground penetrating radar applied to fracture imaging in Gneiss. *Geophysics* 61, 1050–1064.
- Grasmück, M., Green, A.G., 1996. 3-D georadar mapping—looking into the subsurface. *Environ. Eng. Geosci.* II, 195–200.
- Gross, R., Green, A., Holliger, K., Horstmeyer, H., Baldwin, J., 2002. Shallow geometry and displacements on the San Andreas fault near Point Arena based on trenching and 3D georadar surveying. *Geophys. Res. Lett.* 29, 34-1–34-4.
- Jones, I.F., Levy, S., 1987. Signal-to-noise ratio enhancement in multichannel seismic data via the Karhunen–Loève transform. *Geophys. Prospect.* 35, 12–32.
- Lawson, A.C., 1908. The California Earthquake of April 18, 1906. Report of the State Earthquake Investigation Commission. Carnegie Institute Washington Pub. 87. 451 pp.
- Lehmann, F., Boerner, D., Holliger, K., Green, A.G., 2000. Multi-component georadar data: some important implications for data acquisition and processing. *Geophysics* 65, 1542–1552.
- Lehmann, F., Green, A.G., 1999. Semi-automated georadar data acquisition in three dimensions. *Geophysics* 64, 719–731.
- McCalpin, J.P., 1996. Paleoseismology. Academic Press, San Diego. 588 pp.
- Smith, D.G., Jol, H.M., 1995. Wasatch fault (Utah), detected and displacement characterised by ground penetrating radar. *Environ. Eng. Geosci.* I, 489–496.
- Thatcher, W., Marshall, G., Lisowski, M., 1997. Resolution of fault slip along the 470-km-long rupture of the great 1906 San Francisco earthquake and its implications. *J. Geophys. Res.* 102, 5353–5367.
- Working Group on California Earthquake Probabilities, 1999. Earthquake Probabilities in the San Francisco Bay Region: 2000 to 2030—A summary of Findings. U.S. Geological Survey Open File Report 99-517. 60 pp.
- Yeats, R.S., Sieh, K., Allen, C.R., 1997. The Geology of Earthquakes. Oxford Univ. Press, Oxford. 568 pp.